

LPN11-52, TTP11-26, IFIC/11-45

Charge asymmetries of top quarks at hadron colliders revisited

Johann H. Kühn^{a *} and Germán Rodrigo^{a,b †}

^a Institut für Theoretische Teilchenphysik, Karlsruher Institut für Technologie,
D-76133, Karlsruhe, Germany.

^b Instituto de Física Corpuscular,
Consejo Superior de Investigaciones Científicas-Universitat de València,
Parc Científic, E-46980 Paterna (Valencia), Spain.

Abstract

A sizeable difference in the differential production cross section of top- compared to antitop-quark production, denoted charge asymmetry, has been observed at the Tevatron. The experimental results seem to exceed the theory predictions based on the Standard Model by a significant amount and have triggered a large number of suggestions for "new physics". In the present paper the Standard Model predictions for Tevatron and LHC experiments are revisited. This includes a reanalysis of electromagnetic as well as weak corrections, leading to a shift of the asymmetry by roughly a factor 1.1 when compared to the results of the first papers on this subject. The impact of cuts on the transverse momentum of the top-antitop system is studied. Restricting the $t\bar{t}$ system to a transverse momentum less than 20 GeV leads to an enhancement of the asymmetries by factors between 1.3 and 1.5, indicating the importance of an improved understanding of the $t\bar{t}$ -momentum distribution. Predictions for similar measurements at the LHC are presented, demonstrating the sensitivity of the large rapidity region both to the Standard Model contribution and effects from "new physics".

December 12, 2011

*E-mail: johann.kuehn@kit.edu

†E-mail: german.rodrigo@csic.es

1 Introduction

Top quark production at hadron colliders is one of the most active fields of current theoretical and experimental studies [1]. Theoretical predictions [2, 3, 4, 5] for the total production cross section are in very good agreement with experimental results both at the Tevatron at 1.96 TeV [6, 7] and the LHC at 7 TeV [8, 9]. In contrast, sizable differences have been observed between theory predictions [10, 11, 12, 13] for the top quark charge asymmetry and measurements by the CDF and the D0 collaborations [14, 15, 16, 17, 18, 19, 20, 21, 22, 23, 24] at the Tevatron. The discrepancy is particularly pronounced for the subsample of $t\bar{t}$ pairs with large invariant mass, $m_{t\bar{t}} > 450$ GeV, where a 3.4σ effect has been claimed [19]. It is interesting to note, however, that the discrepancy is less prominent in the laboratory frame [19]. These discrepancies have triggered a large number of theoretical investigations, using these results, either to restrict new physics like heavy axiguons [25, 26] or to postulate a variety of new phenomena in the t-channel [27, 28, 29] (see also [30] for a recent review). At the same time the robustness of the leading order QCD prediction has been studied in [31, 32], where it has been argued that next-to-leading (NLL) as well as next-to-next-to leading (NNLL) logarithmic corrections do not significantly modify the leading order result, in agreement with the approach advocated in [11, 12] (Note, however, the large corrections observed in Ref. [33, 34] for the corresponding studies of the $t\bar{t}$ +jet sample). The absence of large corrections in the asymmetry is at variance with the predictions based on Monte-Carlo simulations where the numerator is evaluated in $\mathcal{O}(\alpha_s^3)$ and hence leading order (LO), the denominator also in $\mathcal{O}(\alpha_s^3)$, corresponding to terms of leading plus next-to-leading order. Inclusion of next-to-leading terms in the denominator leads to a reduction by a factor roughly 0.7. A small modification of the Standard Model (SM) prediction arises from inclusion of QED corrections. In Ref. [11] this effect was estimated to lead to an increase of the the asymmetry by a factor 1.09, in a recent analysis [35], however, an enhancement factor of 1.2 has been obtained. Obviously this small increase of the SM prediction for the asymmetry cannot resolve the discrepancy between theory an experiment mentioned above.

In view of this ongoing discussion, a reanalysis of the SM prediction seems appropriate. In this short note we evaluate the QED and weak corrections to the asymmetry, confirming the results of Ref. [35], and compare the SM result with the most recent measurements at Tevatron. Subsequently we study the effect of a cut on the transverse momentum of the $t\bar{t}$ system on the asymmetry. A significant increase is observed, even for a cut as high as 20 GeV by typically a factor 1.3. This applies both at the parton and the hadronic level. Although the implications of this observation for the actual measurement can only be studied quantitatively by a (presently not available) full NNLO simulation, this cut dependence, nevertheless, may serve as an indication of the sensitivity of the asymmetry on details of the analysis.

As noted already in [11, 12], a charge asymmetry may also be defined and observed at the LHC. Since such an effect can only be observed in the small subsample of $q\bar{q}$ induced events, specific kinematic regions must be selected where gluon fusion is suppressed and $q\bar{q}$ - annihilation is enhanced. A particularly sensitive observable is the ratio $A(Y) \equiv (N(y_t > y_{\bar{t}}) - N(y_t < y_{\bar{t}}))/(N(y_t > y_{\bar{t}}) + N(y_t < y_{\bar{t}}))$ with fixed average rapidity $Y \equiv (y_t + y_{\bar{t}})/2$. For large rapidities, say around 2, the SM prediction for $A_{t\bar{t}}(Y)$ amounts up to 0.05 and might well be detected at the LHC.

The quantity $A_{t\bar{t}}(Y)$ is also sensitive to physics beyond the SM. We use axiguons as one particularly illustrative example and study the sensitivity to amplitudes comparable in size to those suggested by recent Tevatron results.

2 Amplitudes and partonic cross section

2.1 QCD asymmetry

As shown in [11, 12], the dominant contribution to the charge asymmetry originates from $q\bar{q}$ annihilation. Specifically, it originates from the interference between the Born amplitudes for $q\bar{q} \rightarrow Q\bar{Q}$ (Fig. 1d) and the part of the one-loop correction, which is antisymmetric under the exchange of quark and antiquark (Fig. 1c) (box and crossed box). To compensate the infrared divergences, this virtual correction must be combined with the interference between initial and final state radiation (Figs. 1a, 1b). Diagrams with triple gluon coupling in both real and virtual corrections give rise to symmetric amplitudes [11, 12] and can be ignored. The corresponding contribution to the rate is conveniently expressed by the absorptive contributions (cuts) of the diagrams depicted in Fig 2.

As a second contribution to the asymmetry we would like to mention “flavor excitation” involving again antisymmetric interference terms of different amplitudes, in this case contributing to quark-gluon scattering as shown in Fig. 3 (amplitudes with triple gluon coupling again don’t give rise to antisymmetric terms). Flavor excitation hardly contributes to the asymmetry at the Tevatron. At the LHC, however, it enhances the asymmetry in suitable chosen kinematical regions, as discussed in Ref. [12].

Compact analytical results for the asymmetric parts of virtual plus soft radiation ($E^g < E_{\text{cut}}^g$) and of hard radiation ($E^g \geq E_{\text{cut}}^g$) can be found in the Appendix of Ref. [11].

Let us recall that the color factors corresponding to Fig. 2a and 2b, after averaging over initial and summing over final states, are given by

$$\begin{aligned} \mathcal{C}_a &= \frac{1}{N_C^2} \text{Tr}(T^a T^b T^c) \text{Tr}(T^a T^c T^b) = \frac{1}{16 N_C^2} (d_{abc}^2 + f_{abc}^2), \\ \mathcal{C}_b &= \frac{1}{N_C^2} \text{Tr}(T^a T^b T^c) \text{Tr}(T^b T^c T^a) = \frac{1}{16 N_C^2} (d_{abc}^2 - f_{abc}^2). \end{aligned} \quad (1)$$

Without color factors the contributions to the differential cross-section from the two- and three-particle cuts in Fig. 2a and 2b are related by

$$d\sigma_a(Q, \bar{Q}) = -d\sigma_b(Q, \bar{Q}). \quad (2)$$

The asymmetric piece thus originates from the d_{abc}^2 term and, in leading order, its form is completely equivalent to the corresponding QED case.

2.2 QED asymmetry

Already at this point we would like to discuss the closely related QED contribution to the asymmetry. Let us start with diagram shown in Fig. 4a following again Ref. [11]. The QCD box leads to a color octet and color singlet configuration, and the latter interferes with $t\bar{t}$ production through the photon. A similar consideration applies to interference between initial and final state radiation. These two contributions are indicated in Fig. 4a by the two cuts, and in combination lead to an additional asymmetric term which can be obtained from the QCD asymmetry through the replacement [11, 12]

$$\frac{\alpha_S}{2} \left(\frac{d_{abc}^2}{4} \right)^2 \rightarrow \alpha_{\text{QED}} Q_t Q_q. \quad (3)$$

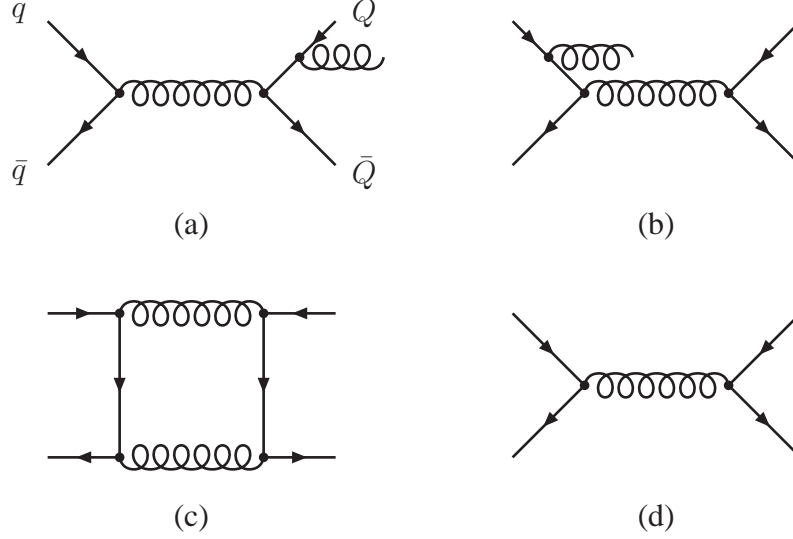


Figure 1: Origin of the QCD charge asymmetry in hadroproduction of heavy quarks: interference of final-state (a) with initial-state (b) gluon bremsstrahlung plus interference of the box (c) with the Born diagram (d). Crossed diagrams are omitted.

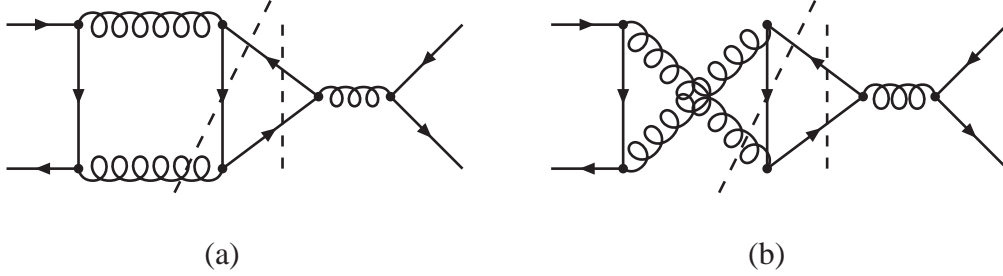


Figure 2: Cut diagrams.

Another QED term originates from the interference between the gluon- γ box with the QCD Born amplitude. Since gluons and photon are distinct fields, two contributions as depicted in Fig. 4b and 4c arise [†]. Each of these contributes with the factor given in Eq. (3). In total the relative factor between QCD and QED asymmetries amounts to

$$f_q^{\text{QED}} = 3 \frac{\alpha_{\text{QED}} Q_t Q_q}{\frac{\alpha_S}{2} \left(\frac{d_{abc}^2}{4} \right)^2} = \frac{\alpha_{\text{QED}}}{\alpha_S} \frac{36}{5} Q_t Q_q \quad (4)$$

for one quark species. Let us, in a first step, assume identical functional dependence of the PDFs for u and d valence quarks in the proton (modulo the obvious factor two) and similarly for antiquarks in the antiproton. Assuming, furthermore, dominance of valence quark-antiquark annihilation in $t\bar{t}$ production, the relative contributions of the $u\bar{u}$ versus $d\bar{d}$ induced reactions to the cross section have to be weighted with the ratio 4:1. The QED asymmetry has to be weighted, furthermore, with relative factors f_u^{QED} and

[†]These small terms had been neglected in [12], in [11] only one of the two had been included. The present result is in agreement with [35]

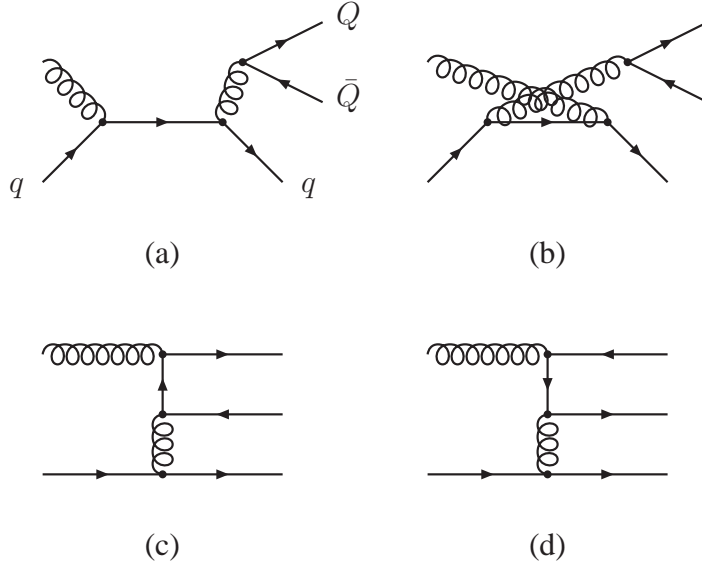


Figure 3: Origin of the QCD charge asymmetry in hadroproduction of heavy quarks through flavor excitation.

f_d^{QED} respectively. The relative QED contribution thus amounts to

$$f_{\text{Tevatron}}^{\text{QED}} = \frac{4f_u^{\text{QED}} + f_d^{\text{QED}}}{5} = \frac{\alpha_{\text{QED}}}{\alpha_S} \frac{56}{25} \approx 0.18, \quad (5)$$

at the Tevatron, and thus to an enhancement of nearly twenty percent of the QCD asymmetry, in good agreement with the more detailed numerical studies presented below and with the results of [35]. Compared to proton-antiproton collisions the relative importance of $u\bar{u}$ versus $d\bar{d}$ annihilation at the LHC is shifted from approximately 4 : 1 to 2 : 1, thus reducing f^{QED} to $f_{\text{LHC}}^{\text{QED}} = (2f_u^{\text{QED}} + f_d^{\text{QED}})/3 \approx 0.13$, which is lower than the result of Eq. (5) by a factor 5/7. The results using standard PDFs are close to these values and will be listed in Sect. 3.2.

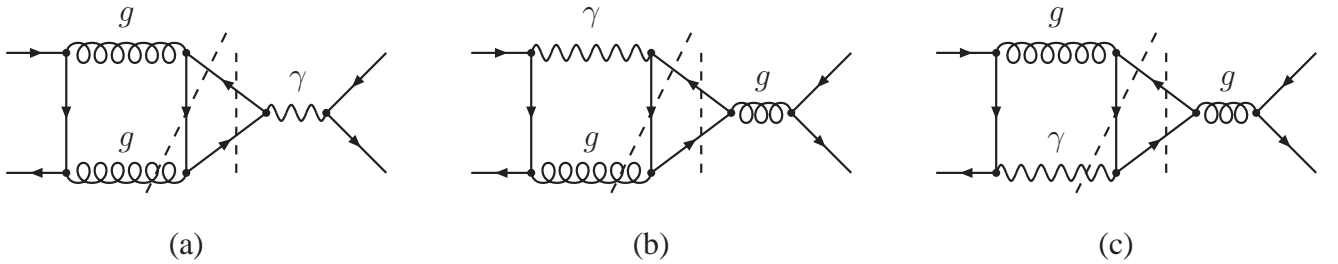


Figure 4: Representative diagrams contributing to the QCD-QED interference term.

2.3 Weak asymmetry

Weak and electromagnetic interactions are of comparable strength at energies characteristic for the Tevatron and the LHC. Hence, contributions similar to those depicted in Figs. 4a, 4b and 4c with the photon replaced by the Z boson should be considered at the same footing. Let us start with the contribution

depicted in Fig. 5a, where the Z boson is off-shell with virtuality $\hat{s} \gg m_Z^2$. The result is obtained [12] from the photon contribution through the replacement

$$Q_t Q_q \rightarrow \frac{(2 I_t - 4 Q_t s_W^2)(2 I_q - 4 Q_q s_W^2)}{16 s_W^2 c_W^2} \frac{1}{1 - m_Z^2/\hat{s}}, \quad (6)$$

with s_W^2 and c_W^2 denoting the squares of the sine and cosine of the weak mixing angle, respectively, and I_q the weak isospin of the relevant quark. Adopting the weighted average similar to Eq. (5) we find

$$f_1^{\text{weak}} = \frac{\alpha_{\text{QED}}}{\alpha_S} \frac{36}{5} \frac{1 - \frac{8}{3} s_W^2}{1 - m_Z^2/\hat{s}} \frac{1}{16 s_W^2 c_W^2} \frac{4(1 - \frac{8}{3} s_W^2) + (-1 + \frac{4}{3} s_W^2)}{5} \approx 4.4 \times 10^{-3}, \quad (7)$$

for the contribution Fig. 5a. Note that, as a consequence of the cancellation between up and down quarks, and the smallness of the weak coupling, this result is smaller by more than a factor 10 than the corresponding photonic result. For proton-proton collision f_1^{weak} is further reduced down to 7×10^{-4} and thus is completely negligible.

It is tempting to estimate the contributions from diagrams 5b and 5c along the same lines. Independently of any detailed considerations the same compensation between u - and d -quark contributions will arise, and in the limit $m_Z^2 \ll \hat{s}$, and assuming that final states with real Z radiation are included in the sample of $t\bar{t}$ events, the analogs of Figs. 5b and 5c will contribute identically to Fig. 5a, enhancing the correction from 0.5% to 1.5%. Alternatively, one may perform an explicit calculation of Figs. 5b and 5c, allowing for a separation of real and virtual Z boson radiation.

Let us, finally mention that contributions to the asymmetry involving the squared electroweak amplitude $q\bar{q} \xrightarrow{\gamma, Z} t\bar{t}$ are of order $\alpha_{\text{QED}}^2/\alpha_S^2$ and thus at most of $\mathcal{O}(1\%)$. Furthermore, if we would include terms of order $\alpha_{\text{QED}}^2/\alpha_S^2$ into consideration, terms of order $\alpha_S^2 \alpha_{\text{QED}}$ in the total cross-section, i.e. electroweak corrections to $t\bar{t}$ production (leading to corrections of comparable size [36, 37, 38, 39, 40]) should be included as well. Since even the NLO QCD corrections to the asymmetry of $\mathcal{O}(\alpha_S)$ have not been evaluated to date, it seems unnecessary to include these $\mathcal{O}(\alpha_{\text{QED}}^2)$ terms into consideration.

Indeed, considering the large positive NLO QCD corrections to the cross-section amounting to about 30% at the Tevatron, it seems plausible to assign a comparable uncertainty to the asymmetry. However, in agreement with [11, 12, 31, 32], we shall assume that the central value of the asymmetry will not be shifted by the large corrections, in other words, that symmetric and antisymmetric parts of the cross-section are shifted by the same factor.

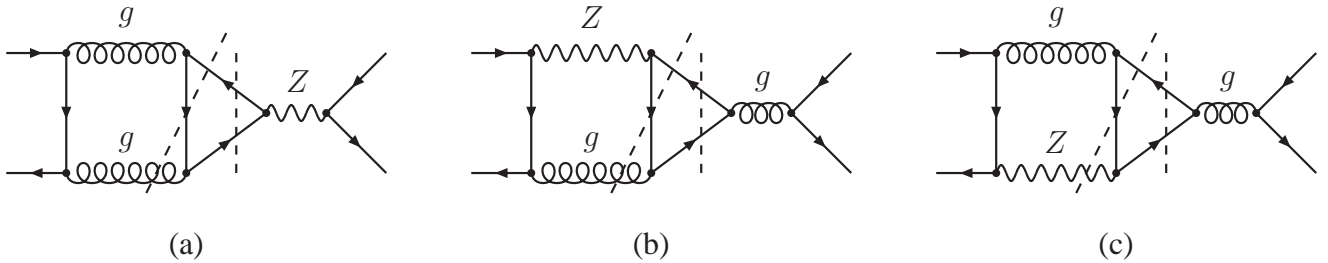


Figure 5: Representative diagrams contributing to the QCD-weak interference term.

2.4 Numerical results at the partonic level

Results for the angular distribution of the antisymmetric part of the cross section are shown in Fig. 6 (left plots) for fixed partonic center of mass energies, and divided by the total $q\bar{q}$ induced cross-section:

$$\hat{A}(\cos \hat{\theta}) = \frac{1}{\sigma_{q\bar{q}}} \frac{d\sigma_A(\cos \hat{\theta})}{d \cos \hat{\theta}}. \quad (8)$$

QED induced terms are shown separately for u and d quarks, as well as the partonic asymmetry generated by $q\bar{q}$ collisions. The QED generated asymmetries for u and d quarks follows the proportionality factor in Eq. (4), amounting to $\alpha_{\text{QED}}/\alpha_S \frac{36}{5} Q_t Q_q \approx 0.38 Q_q$. The piece generated by $q\bar{q}$ collisions (flavor excitation) remains small in the whole kinematic region of interest.

At this point it is instructive to study the effect of cuts on gluon emission, which lead to an enhancement of the asymmetry. To understand the origin of this phenomenon, let us in a first step recall that the inclusive asymmetry is positive, which can be qualitatively understood from the requirement that the final state configuration with minimal modification of the color field is favored, corresponding to minimal change of the direction of the color source. On the other hand, if one request a hard gluon in the final state, this configuration is more probable for backward going top quarks, thus emitting hard bremsstrahlung. Hence, for events with tagged hard gluons a negative charge asymmetry is expected. Conversely, one expects a sizable increase of the inclusive asymmetry, if one cuts on events with real gluon emission. This is demonstrated in Fig. 6 (right plots) where the dashed and the dotted curves are obtained for a cut on the transverse momentum of the top quark pair $p_{\perp}^{t\bar{t}} < p_{\perp}^{\text{max}}$ with p_{\perp}^{max} chosen differently for different \hat{s} . We observe an increase of the asymmetry by a significant amount. The effect is strongly dependent on the precise value of p_{\perp}^{max} and becomes more pronounced at larger \hat{s} , a consequence of the relatively larger amount of real radiation in the fully inclusive sample.

The energy dependence of the integrated asymmetry (again normalized relative to the Born cross-section $\sigma(q\bar{q} \rightarrow t\bar{t})$,

$$\hat{A} = \int_0^1 \hat{A}(\cos \hat{\theta}) d \cos \hat{\theta} - \int_{-1}^0 \hat{A}(\cos \hat{\theta}) d \cos \hat{\theta} \quad (9)$$

is displayed in Fig. 7. As in Fig. 6, the left plot in Fig. 7 show the pure QCD asymmetry generated by $q\bar{q}$ and $q\bar{q}$ events, and the QCD-QED mixed asymmetry for u and d initial quarks. A rapid increase of the asymmetry is observed in the region very close to threshold, a consequence of the S-wave–P-wave interference of the asymmetry. The right plot in Fig. 7 illustrates the effect on the QCD induced asymmetry from introducing a cut on the transverse momentum of the top quark pair $p_{\perp}^{t\bar{t}}$. Again a sizable increase of \hat{A} is observed, which depends strongly on the choice of the cut.

We use the following values for the top quark mass $M_t = 173.3(1.1)$ GeV [41], the strong coupling $\alpha_S(M_Z) = 0.1184(7)$ [42], the QED coupling $\alpha_{\text{QED}}(M_Z) = 1/127$, and the square of the sine of the weak mixing $s_W^2 = 0.23$. The renormalization scale in Fig. 6 and Fig. 7 has been set to the partonic center of mass energy, $\mu = \sqrt{\hat{s}}$.

3 Hadronic collisions

3.1 Generalities

The asymmetry can, in principle, be studied in more detail by measuring in addition $m_{t\bar{t}}$, the invariant mass of the $t\bar{t}$ system, and its transverse momentum, which is balanced by the transverse momentum of an additionally radiated gluon. Controlling both observables together with the asymmetry would provide detailed information on the production dynamics. Although such a measurement is only possible with large statistics, a first step into this direction has been performed by the CDF collaboration by separating events with invariant mass of the $t\bar{t}$ -system above and below 450 GeV. However, for a complete investigation the statistical precision is far too small.

In the following we will present in a first step, our predictions for the Tevatron, subsequently for the LHC. We will include the update on the electromagnetic and weak corrections, discuss the implications of a $p_{\perp}^{t\bar{t}}$ cut on the asymmetry, and compare our results to the most recent experimental results. In a second step we present detailed predictions for the LHC and identify kinematic regions where the charge asymmetry could be observed. In view of the indications at the Tevatron for a sizable excess of the asymmetry, we then investigate the implications for the charge asymmetry at the LHC in two benchmark scenarios beyond the SM.

Different choices of parton distribution functions of the MSTW2008 set [43] are used to obtain the theoretical predictions of the asymmetry in hadronic collisions, specifically we consider MSTW2008LO and MSTW2008NLO. The dependence of the asymmetry on the choice of PDFs is, however, small. The factorization and renormalization scales are varied between $\mu = m_t/2$ and $\mu = \sqrt{\hat{s}}$. This dependence gives the bulk of the estimated theoretical error because the asymmetry is proportional to $\alpha_S(\mu)$. The variation of the top mass within its experimental error is also considered; its effect on the asymmetry is also small.

3.2 Tevatron

Let us start with our updated predictions for the Tevatron. Assuming that the rapidities of t and \bar{t} have been measured simultaneously, one defines the asymmetry

$$A_{t\bar{t}}(Y) = \frac{N(y_t > y_{\bar{t}}) - N(y_{\bar{t}} > y_t)}{N(y_t > y_{\bar{t}}) + N(y_{\bar{t}} > y_t)}, \quad (10)$$

where $Y = (y_t + y_{\bar{t}})/2$ has been fixed. The results as a function of Y are shown in Fig. 8. An almost flat $A_{t\bar{t}}(Y)$ of around 8% is observed. Two versions of the integrated asymmetry have been introduced in Refs. [10, 11, 12]: the forward–backward asymmetry in the laboratory frame

$$A_{\text{lab}} = \frac{N(y_t > 0) - N(y_t < 0)}{N(y_t > 0) + N(y_t < 0)} = \frac{N(y_t > 0) - N(y_{\bar{t}} > 0)}{N(y_t > 0) + N(y_{\bar{t}} > 0)}, \quad (11)$$

and the asymmetry in the $t\bar{t}$ rest frame

$$A_{t\bar{t}} = \frac{N(y_t > y_{\bar{t}}) - N(y_{\bar{t}} > y_t)}{N(y_t > y_{\bar{t}}) + N(y_{\bar{t}} > y_t)}. \quad (12)$$

Table 1: Predicted asymmetries in the laboratory A_{lab} and the $t\bar{t}$ rest-frame $A_{t\bar{t}}$ at Tevatron. And relative amount of $u\bar{u}$, $d\bar{d}$ gg initiated processes. Predictions are given also for samples with the top quark pair invariant mass $m_{t\bar{t}}$ above and below 450 GeV.

laboratory	A_{lab}	$m_{t\bar{t}} < 450 \text{ GeV}$	$m_{t\bar{t}} > 450 \text{ GeV}$
QCD	0.047 (7)	0.024 (2)	0.084 (9)
QED $u\bar{u}$	0.0094	0.0047	0.0174
QED $d\bar{d}$	-0.0008	-0.0004	-0.0012
weak $u\bar{u}$	0.0011	0.0006	0.0021
weak $d\bar{d}$	-0.0003	-0.0002	-0.0005
SM	0.056 (7)	0.029 (2)	0.102 (9)
MCFM [19]	0.038 (6)		
$t\bar{t}$ rest frame	$A_{t\bar{t}}$	$m_{t\bar{t}} < 450 \text{ GeV}$	$m_{t\bar{t}} > 450 \text{ GeV}$
QCD	0.072 (9)	0.052 (4)	0.106 (11)
QED $u\bar{u}$	0.0145	0.0101	0.0219
QED $d\bar{d}$	-0.0012	-0.0010	-0.0015
weak $u\bar{u}$	0.0018	0.0012	0.0027
weak $d\bar{d}$	-0.0005	-0.0004	-0.0006
SM	0.087 (10)	0.062 (4)	0.128 (11)
MCFM [19]	0.058 (9)	0.040 (6)	0.088 (13)
relative amount	inclusive	$m_{t\bar{t}} < 450 \text{ GeV}$	$m_{t\bar{t}} > 450 \text{ GeV}$
$u\bar{u}$	0.78	0.76	0.82
$d\bar{d}$	0.14	0.15	0.11
gg	0.08	0.09	0.07

Results for both of them are listed in Table 1. This Table also lists separately the contributions from pure QCD and from QED, the latter again separated for up and down quark. The relative QED contribution $(\text{QED } u\bar{u} + \text{QED } d\bar{d}) / \text{QCD}$ as obtained from Table 1 is close to 0.18 for all the cases considered and thus in agreement with the expectations based on Eq. (5). Similarly, we also give the results for the weak terms in the asymmetry, using the approximation $m_Z^2 \ll \hat{s}$. Note that the weak contribution is strongly suppressed, even in comparison with the QED piece, and hence can be safely treated in this approximation. The relative contribution of gg , $u\bar{u}$ and $d\bar{d}$ initiated top quarks is also listed in this Table. Due to the deviation of the relative amount of u - and d - contributions from the simple approximation 4 : 1 we find a slight deviation from Eq. (5). The overall factor 1.21 is consistent with [35].

In view of the strong dependence of the asymmetry on the invariant mass of the $t\bar{t}$ system, evident already from Figs. 6 and 7, we also study the dependence of the integrated asymmetries on a cut on the invariant mass of the $t\bar{t}$ system. Separating the events into two samples with $m_{t\bar{t}}$ smaller and larger than 450 GeV respectively, the average value $A_{t\bar{t}} = 0.087(10)$ moves down to 0.062(4) and up to 0.128(11) for the two choices. A similar behaviour is observed for the asymmetry A_{lab} defined in the laboratory frame.

It is interesting to compare these results with those based on a Monte Carlo prediction [19] based on MCFM [44]. The enhancement factor of the SM result in Table 1 compared to MCFM of about 1.5 is easily understood: a factor 1.2 originates from the inclusion of QED effects, that had been discussed in [12] and improved in [35]. Another factor of about 1.3 originates from normalizing with respect to the

Born cross-section instead of the NLO result. Since the asymmetric part of the cross-section is presently known to LO only we consider the normalization to the LO cross-section more plausible [11, 12, 31, 32].

For illustration, we compare these theoretical results in the SM with the most recent measurements at Tevatron [14, 17, 18, 19] as summarized in Table 2. Predictions and results are shown both for A_{lab} and $A_{t\bar{t}}$ and, when available, also split into two samples with $m_{t\bar{t}}$ larger and smaller than 450 GeV, and with $|\Delta y| = |y_t - y_{\bar{t}}|$ larger and smaller than 1. We note the nearly universal factor ~ 1.5 between our result (SM) and the Monte Carlo simulation (MCFM / MC@NLO), which slightly softens the tension between theory and experiment. The errors from the choice of PDFs and factorization scale are small, the dominant uncertainty arises from varying the renormalization scale and hence the value of α_S . If we would take the difference between LO and NLO prediction for the total production cross-section as measure of the theory uncertainty, the error would increase up to $\pm 30\%$. A graphical illustration of the results in terms of the "pull" (measured in standard deviations) is shown in Fig. 9 (errors from theory and experiment are combined quadratically. For the results which refer to "reconstruction level" we use the MCFM / MC@NLO results, multiplied by a factor 1.5.) The systematic upward shift of all but two Tevatron results is evident. The highest discrepancy, as has extensively been discussed in the literature, occurs for samples with $m_{t\bar{t}} > 450$ GeV and the charge asymmetry defined in the $t\bar{t}$ rest frame. Also shown in this Figure are preliminary results from CMS [45] and ATLAS [46] with a slight pull in the opposite direction.

Let us now investigate the impact of cuts on hard gluon (and photon) radiation on $A_{t\bar{t}}(Y)$. The dotted and dashed curves in Fig. 8 show the effect of a cut on $p_{\perp}^{t\bar{t}}$ for values of $p_{\perp}^{\text{max}} = 10$ GeV and 20 GeV, respectively. An increase of the asymmetry by more than a factor 1.5 in the central region is observed for the most restrictive choice of 10 GeV, and even a fairly loose $p_{\perp}^{\text{max}} = 20$ GeV modifies the asymmetry by up to a factor 1.3. The dependence on Y , the average rapidity of the t and \bar{t} , is less flat than in the inclusive case. Similar enhancement factors are therefore also present in the integrated asymmetries, as displayed in Table 3. A fairly similar behaviour is observed if cuts on both $m_{t\bar{t}}$ and $p_{\perp}^{t\bar{t}}$ are imposed, as shown in the third and fourth column of Table 3. Note that the p_{\perp} distribution of the $t\bar{t}$ -system, as measured by the D0 Collaboration, seems to be at variance with the prediction based on the NLO Monte Carlo simulation [47] (Leading order simulations like PYTHIA [48] are by construction not able to correctly predict the asymmetry.) Considering the fact that in the course of the experimental analysis $t\bar{t}$ events are separated into a sample with four jets (of p_{\perp} larger than 20 GeV) and a sample with five and more jets (with different reconstruction algorithms and efficiencies) it seems important to verify that one nevertheless arrives at an unbiased inclusive sample.

3.3 LHC

As discussed in [10, 11, 12] it is possible to investigate the charge asymmetry also in proton-proton collisions at the LHC, exploiting the small $t\bar{t}$ sample produced in annihilation of valence quarks and antiquarks from the sea. As illustrated in Fig. 10 production of quarks with larger rapidities will be preferred, antitop quarks will be produced more frequently at smaller rapidities. This observation suggests to define the cut-dependent asymmetries

$$A_C^{\text{in}}(y_C) = \frac{N(|y_{\bar{t}}| \leq y_C) - N(|y_t| \leq y_C)}{N(|y_t| \leq y_C) + N(|y_{\bar{t}}| \leq y_C)} \quad (13)$$

Table 2: Recent experimental measurements of the asymmetry in the laboratory A_{lab} and in the $t\bar{t}$ rest frame $A_{t\bar{t}}$ at Tevatron. Results with $|\Delta y| = |y_t - y_{\bar{t}}|$ larger or smaller than 1 are also summarized. Numbers with * refer to ‘‘reconstruction level’’ [19, 14], the others to parton level.

laboratory	A_{lab}	$m_{t\bar{t}} < 450 \text{ GeV}$	$m_{t\bar{t}} > 450 \text{ GeV}$
SM (this work)	0.056 (7)	0.029 (2)	0.084 (9)
CDF [19] 5.3 fb ⁻¹ (1+jet)	0.150 ± 0.050 ± 0.024	0.059 (34)*	0.103 (49)*
MCFM/MC@NLO* [19]	0.038 (6)	-0.008 (5)*	0.022 (7)*
$t\bar{t}$ rest frame	$A_{t\bar{t}}$	$m_{t\bar{t}} < 450 \text{ GeV}$	$m_{t\bar{t}} > 450 \text{ GeV}$
SM (this work)	0.087 (10)	0.062 (4)	0.128 (11)
CDF [18] 5.1 fb ⁻¹ (dilep)	0.42 ± 0.15 ± 0.05		
CDF [19] 5.3 fb ⁻¹ (1+jet)	0.158 ± 0.072 ± 0.017	-0.116 ± 0.146 ± 0.047	0.475 ± 0.101 ± 0.049
CDF [17] (combined)	0.20 ± 0.07 ± 0.02		
MCFM [19]	0.058 (9)	0.040 (6)	0.088 (13)
D0 [14] 5.4 fb ⁻¹ (1+jet)	0.196 (65)	0.078 (48)*	0.115 (60)*
MC@NLO [14]	0.050 (10)	0.013 (6)*	0.043 (13)*
$t\bar{t}$ rest frame $ \Delta y < 1$	$A_{t\bar{t}}$	$m_{t\bar{t}} < 450 \text{ GeV}$	$m_{t\bar{t}} > 450 \text{ GeV}$
SM (this work)	0.057 (4)	0.053 (4)	0.069 (5)
CDF [19] 5.3 fb ⁻¹ (1+jet)	0.026 ± 0.104 ± 0.056		
MCFM [19]	0.039 (6)		
D0 [14] 5.4 fb ⁻¹ (1+jet)	0.061 (41)*		
MC@NLO [14]	0.014 (6)*		
$t\bar{t}$ rest frame $ \Delta y > 1$	$A_{t\bar{t}}$	$m_{t\bar{t}} < 450 \text{ GeV}$	$m_{t\bar{t}} > 450 \text{ GeV}$
SM (this work)	0.193 (15)	0.149 (8)	0.209 (15)
CDF [19] 5.3 fb ⁻¹ (1+jet)	0.611 ± 0.210 ± 0.147		
MCFM [19]	0.123 (18)		
D0 [14] 5.4 fb ⁻¹ (1+jet)	0.213 (97)*		
MC@NLO [14]	0.063 (16)*		

and

$$A_C^{\text{out}}(y_C) = \frac{N(|y_t| > y_C) - N(|y_{\bar{t}}| > y_C)}{N(|y_t| > y_C) + N(|y_{\bar{t}}| > y_C)}, \quad (14)$$

which serve to characterize the depletion of top quarks in the central region ($A_C^{\text{in}}(y_C) > A_C^{\text{out}}(y_C)$ for $y_C < 0.7$ approximately [10]), and their enhancement at larger rapidities ($A_C^{\text{in}}(y_C) < A_C^{\text{out}}(y_C)$ for $y_C > 0.7$). Note that we have defined $A_C^{\text{in}}(y_C)$ in Eq. (13) with the opposite sign than in Ref. [10, 49, 50] such that both $A_C^{\text{in}}(y_C)$ and $A_C^{\text{out}}(y_C)$ are positive in the SM. The dependence of A_C^{in} and A_C^{out} on y_C is shown in Fig. 11 for $\sqrt{s} = 7 \text{ TeV}$ (left plot) and 14 TeV (right plot). As one can observe in these Figures, A_C^{out} is much larger than A_C^{in} at large values of the rapidity cut y_C . This is because the central region is dominated by gluon fusion processes, while the sample with large rapidities has a larger relative content of $q\bar{q}$ initiated events. The statistical significance of both observables is, however, very similar [51] because the larger size of the asymmetry A_C^{out} with respect to A_C^{in} is compensated by the lower rate of events at larger rapidities. We consider also the cut-independent charge asymmetries

$$A_C^\eta = \frac{N(\Delta_\eta > 0) - N(\Delta_\eta < 0)}{N(\Delta_\eta > 0) + N(\Delta_\eta < 0)} \quad (15)$$

Table 3: SM asymmetries in the laboratory A_{lab} and the $t\bar{t}$ rest-frame $A_{t\bar{t}}$ for different cuts in $p_{\perp}^{t\bar{t}}$.

laboratory	A_{lab}	$m_{t\bar{t}} < 450 \text{ GeV}$	$m_{t\bar{t}} > 450 \text{ GeV}$
$p_{\perp}^{t\bar{t}} < 10 \text{ GeV}$	0.090 (12)	0.047 (3)	0.161 (16)
$p_{\perp}^{t\bar{t}} < 20 \text{ GeV}$	0.076 (10)	0.040 (3)	0.137 (13)
$t\bar{t}$ rest frame	$A_{t\bar{t}}$	$m_{t\bar{t}} < 450 \text{ GeV}$	$m_{t\bar{t}} > 450 \text{ GeV}$
$p_{\perp}^{t\bar{t}} < 10 \text{ GeV}$	0.136 (16)	0.097 (8)	0.201 (19)
$p_{\perp}^{t\bar{t}} < 20 \text{ GeV}$	0.115 (13)	0.082 (7)	0.171 (16)

Table 4: SM cut-independent asymmetries A_{η} and A_y at different LHC energies.

	A_C^{η}	A_C^y
LHC 7 TeV	0.0136 (8)	0.0115 (6)
LHC 8 TeV	0.0122 (7)	0.0102 (5)
LHC 10 TeV	0.0101 (6)	0.0082 (4)
LHC 12 TeV	0.0087 (5)	0.0068 (3)
LHC 14 TeV	0.0077 (4)	0.0059 (3)
LHC 7 TeV CMS [45] 1.09 fb^{-1}	-0.016 ± 0.030	-0.013 ± 0.026
LHC 7 TeV ATLAS [46] 0.7 fb^{-1}	$^{+0.010}_{-0.019}$	$^{+0.026}_{-0.021}$
		$-0.024 \pm 0.016 \pm 0.023$

and

$$A_C^y = \frac{N(\Delta_y > 0) - N(\Delta_y < 0)}{N(\Delta_y > 0) + N(\Delta_y < 0)}, \quad (16)$$

where $\Delta_{\eta} = |\eta_t| - |\eta_{\bar{t}}|$ and $\Delta_y = |y_t| - |y_{\bar{t}}|$, which have been used in the recent CMS [45] and ATLAS [46] analysis. The SM predictions for the integrated asymmetries are listed Table 4 for different center-of-mass energies of the LHC, together with the experimental results for $\sqrt{s} = 7 \text{ TeV}$. Both experiments obtain negative asymmetries, although compatible with the SM prediction within uncertainties.

Top quark production in proton-proton collisions is dominated by gluon fusion, which, in turn, is dominant in the central region. Conversely, quark-antiquark annihilation will be more enriched for events with $t\bar{t}$ at larger rapidities (and larger $m_{t\bar{t}}$). This suggests to employ the definition of Eq. (10), which is essentially the asymmetry in the $t\bar{t}$ rest frame, also for the present case, and concentrate on $t\bar{t}$ events at large rapidities. The prediction for $A_{t\bar{t}}(Y)$ is shown in Fig. 12 for $\sqrt{s} = 7 \text{ TeV}$ (left plot) and 14 TeV (right plot). Note that $A_{t\bar{t}}(Y)$ is now, by construction, an antisymmetric function of Y . Since most of the charge asymmetry is concentrated at large rapidities the statistical significance of any measurement will be enhanced, if the sample is restricted to larger rapidities. Let us therefore define the quantity

$$A_{t\bar{t}}^{\text{cut}}(Y_{\text{cut}}) = \frac{N(y_t > y_{\bar{t}}) - N(y_{\bar{t}} > y_t)}{N(y_t > y_{\bar{t}}) + N(y_{\bar{t}} > y_t)}, \quad (17)$$

where $(y_t + y_{\bar{t}})/2 > Y_{\text{cut}}$ [‡]. The prediction for $A_{t\bar{t}}^{\text{cut}}(Y_{\text{cut}})$ is shown in Fig. 13 for $\sqrt{s} = 7 \text{ TeV}$ (left upper plot) and 14 TeV (right upper plot). Note that the prediction includes QED and weak corrections, which amount to roughly a factor 1.1. To estimate the statistical sensitivity of such a measurement, the

[‡]The asymmetry $A_{t\bar{t}}^{\text{cut}}(Y_{\text{cut}})$ of the sample with $(y_t + y_{\bar{t}})/2 < -Y_{\text{cut}}$ is of the same magnitude but of opposite sign. Both samples can be combined to enhance the statistical significance of the measurement by introducing a flip of sign in the definition of $A_{t\bar{t}}^{\text{cut}}(Y_{\text{cut}})$ for events with $(y_t + y_{\bar{t}})/2 < -Y_{\text{cut}}$.

cross section for events with $t\bar{t}$ at large rapidities $|(y_t + y_{\bar{t}})/2| > Y_{\text{cut}}$ is shown in Fig. 13 (lower plots) as a function of Y_{cut} . Using $\sqrt{s} = 7$ and an integrated luminosity of 20 fb^{-1} as example, more than 4×10^5 events are expected for $Y_{\text{cut}} = 1$. Even allowing for a significant reduction of the sample by small efficiencies, the asymmetry $A_{t\bar{t}}^{\text{cut}}(Y_{\text{cut}})$ of more than 2% could be observed by experiment.

As discussed before, cuts on $p_{\perp}^{t\bar{t}}$ and $m_{t\bar{t}}$ may lead to a significant modification of the asymmetry. The impact of a cut $p_{\perp}^{t\bar{t}} < 20 \text{ GeV}$ on $A_{t\bar{t}}(Y)$ and $A_{t\bar{t}}^{\text{cut}}(Y_{\text{cut}})$ is shown Figs. 12 and 13 (upper plots) as dashed curves. Numerical results for the integrated pair charge asymmetry with $Y_{\text{cut}} = 0.7$ are listed in Table 5 for the inclusive sample, $A_{t\bar{t}}^{\text{cut}}(Y_{\text{cut}} = 0.7)$, and for subsamples with $m_{t\bar{t}}$ larger and smaller than 450 GeV. By definition $A_{t\bar{t}}^{\text{cut}}(Y_{\text{cut}} = 0) = A_C^y$, for which results are listed in Table 4.

Table 5: SM integrated pair charge asymmetry at different LHC energies for $Y_{\text{cut}} = 0.7$, for the inclusive sample, $A_{t\bar{t}}^{\text{cut}}(Y_{\text{cut}} = 0.7)$, and for subsamples with $m_{t\bar{t}}$ larger and smaller than 450 GeV.

	$A_{t\bar{t}}^{\text{cut}}(Y_{\text{cut}} = 0.7)$	$m_{t\bar{t}} < 450 \text{ GeV}$	$m_{t\bar{t}} > 450 \text{ GeV}$
LHC 7 TeV	0.0203 (8)	0.0148 (5)	0.0263 (8)
LHC 8 TeV	0.0178 (6)	0.0128 (4)	0.0224 (7)
LHC 10 TeV	0.0142 (5)	0.0104 (4)	0.0174 (5)
LHC 12 TeV	0.0117 (4)	0.0085 (3)	0.0143 (4)
LHC 14 TeV	0.0100 (4)	0.0075 (3)	0.0121 (4)

4 Charge asymmetry beyond the SM at the LHC

As noted in [10], the asymmetry induced by a ‘‘conventional’’ axigluon G , i.e. with identical axial-vector coupling g_S for all quarks and assuming $m_G > 2m_t$, is negative. This has led to stringent bounds on m_G [25]. On the other hand the apparent positive excess as observed at the Tevatron has led to numerous suggestions for physics beyond the SM which, however, are difficult to reconcile with other experimental facts (For a recent discussion see e.g. [30]). On the contrary, both measurements at CMS [45] and ATLAS [46] point towards negative asymmetries, although still with large uncertainties and compatible with the SM. Independently of these theoretical and experimental considerations it will be interesting to investigate the same phenomena at the LHC. As discussed previously in [11] (see e.g. Figs. 11 and 12) it is possible to identify kinematic regions where $q\bar{q}$ annihilation into $t\bar{t}$ is comparable or even larger than gluon fusion, and the charge asymmetry is suitable to probe new physics beyond the SM in that kinematical regions. We do not try in this section to focus on a particular model that would fit better the Tevatron anomaly and then extrapolate that model to the LHC. Rather, we try to investigate the power of the charge asymmetry defined in Eq. (17) to discriminate among two of the simplest models giving rise to a BSM charge asymmetry, one of them giving a positive excess, and another one leading to a negative contribution.

The most recent measurements at the LHC of the dijet cross-section [52, 53] impose stringent constraints on axigluon masses below 3 TeV. Still, those limits can be relaxed when considering top quark pair production in models in which the coupling of the axigluon vector boson to light quarks is much smaller than the coupling to the top quark. As the simplest case, however, we consider here the case where the extra gauge boson couples with the same strength to light and top quarks, in two different scenarios: a flavour universal case (octet U), i.e. vector-axial couplings to light and top quarks are equal

to the strong coupling g_S multiplied by a factor 1.8, $g_A^q = g_A^t = 1.8$, and a flavour non-universal case (octet A) with vector-axial couplings to light and top quarks of the opposite sign [25], $g_A^q = -g_A^t = 1.8$. The latter naturally produces positive contributions to the charge asymmetry, and has been advocated as one of the possible solutions to the Tevatron anomaly. The former gives a negative contribution to the charge asymmetry, and is disfavored by most of the Tevatron measurements, but still compatible with some of the measurements within 2σ (see Fig. 9). In both cases we consider an axigluon mass of 3 TeV as benchmark model.

The pair charge asymmetries $A_{t\bar{t}}(Y)$ and $A_{t\bar{t}}(Y_{\text{cut}})$ for both benchmark models and for $\sqrt{s} = 7$ TeV and 14 TeV are shown in Fig. 14 in comparison with the SM prediction. We also provide predictions for samples with a large invariant mass of the top quark pair $m_{t\bar{t}} > 450$ GeV. As expected, the BSM contribution to the asymmetry in the octet U model is negative, and it is positive in the octet A model. For low values of Y_{cut} the integrated asymmetry $A_{t\bar{t}}(Y_{\text{cut}})$ is almost twice the asymmetry in the SM for octet A, and almost vanishes for octet U. Introducing a cut in $m_{t\bar{t}}$ also enhances the size of the asymmetry, as in the SM, and in particular for large values of Y_{cut} .

5 Summary and Conclusions

The Standard Model predictions for the top quark charge asymmetry have been reanalysed including QED and weak corrections. For proton-antiproton collisions QED terms lead to an enhancement by a factor of about 1.2 in agreement with [40], and slightly larger than the factor 1.1 obtained in [11]. In total, our prediction is larger than the NLO Monte Carlo results by a factor around $1.5 \approx 1.2 \times 1.3$, where the second factor arises from the different normalisation prescription.

The effect of a cut on the $t\bar{t}$ transverse momentum has been studied and shown to lead to a significant enhancement of the asymmetry. As a characteristic example we study a $p_{\perp}^{t\bar{t}}$ -cut of 20 GeV which leads — for the Tevatron — to an enhancement of around 1.3, and even more for more restrictive cuts.

Various definitions of observables are presented which are sensitive to the charge asymmetry and which can be measured at the LHC. The quantity $A_{t\bar{t}}(Y)$, which measures the forward–backward asymmetry with respect to the average rapidity of top and antitop quark, can amount up to 7%, if the large Y -region is selected. Considering the large statistics expected for the LHC in the near future, this asymmetry (and its integrated version) might soon be measurable at LHC experiments. We have also provided predictions in two benchmark axigluon-like models for these new observables.

Acknowledgements

Work supported in part by the Research Executive Agency (REA) of the European Union under the Grant Agreement number PITN-GA-2010-264564 (LHCPhenoNet), by the Ministerio de Ciencia e Innovación under Grants No. FPA2007-60323, FPA2011-23778 and PR2010-0481, by CPAN (Grant No. CSD2007-00042), by the Generalitat Valenciana under Grant No. PROMETEO/2008/069, by the BMBF under contract 05HT4VKAI3, and the Sonderforschungsbereich/Transregio SFB/TR9 ”Computational Particle Physics”. G.R. acknowledges hospitality at the Institut für Theoretische Teilchenphysik of the Karlsruher

Institut für Technologie during the completion of this work. We thank J. Wagner-Kuhr, T. Peiffer, T. Chwalek, C. Boeser and J. Huston for very usefull discussions.

References

- [1] A. B. Galtieri *et al.* [CDF and D0 Collaboration], [arXiv:1109.2163 [hep-ex]].
- [2] V. Ahrens, A. Ferroglia, B. D. Pecjak, L. L. Yang, Phys. Lett. **B703** (2011) 135-141 [arXiv:1105.5824 [hep-ph]].
- [3] M. Cacciari, S. Frixione, M. L. Mangano, P. Nason, G. Ridolfi, JHEP **0809** (2008) 127 [arXiv:0804.2800 [hep-ph]].
- [4] S. Moch, P. Uwer, Phys. Rev. **D78** (2008) 034003 [arXiv:0804.1476 [hep-ph]].
- [5] N. Kidonakis, Phys. Rev. D **82** (2010) 114030 [arXiv:1009.4935 [hep-ph]].
- [6] T. Aaltonen *et al.* [The CDF Collaboration], Phys. Rev. **D82** (2010) 052002 [arXiv:1002.2919 [hep-ex]].
- [7] V. M. Abazov *et al.* [D0 Collaboration], Phys. Lett. **B679** (2009) 177-185 [arXiv:0901.2137 [hep-ex]].
- [8] [ATLAS Collaboration], ATLAS-CONF-2011-140, ATLAS-CONF-2011-121, ATLAS-CONF-2011-119, ATLAS-CONF-2011-108, ATLAS-CONF-2011-100.
- [9] [CMS Collaboration], CMS-PAS-TOP-11-007, CMS-PAS-TOP-11-006, CMS-PAS-TOP-11-005, CMS-PAS-TOP-11-003.
- [10] O. Antuñano, J. H. Kühn, G. Rodrigo, Phys. Rev. **D77** (2008) 014003 [arXiv:0709.1652 [hep-ph]].
- [11] J. H. Kühn, G. Rodrigo, Phys. Rev. **D59** (1999) 054017 [hep-ph/9807420].
- [12] J. H. Kühn, G. Rodrigo, Phys. Rev. Lett. **81** (1998) 49-52 [hep-ph/9802268].
- [13] M. T. Bowen, S. D. Ellis, D. Rainwater, Phys. Rev. **D73** (2006) 014008 [hep-ph/0509267].
- [14] V. M. Abazov *et al.* [D0 Collaboration], [arXiv:1107.4995 [hep-ex]].
- [15] [D0 Collaboration], D0 Note 6062.
- [16] V. M. Abazov *et al.* [D0 Collaboration], Phys. Rev. Lett. **100** (2008) 142002 [arXiv:0712.0851 [hep-ex]].
- [17] T. Schwarz *et al.* [CDF Collaboration], CDF Note 10584.
- [18] [CDF Collaboration], CDF Note 10436.
- [19] T. Aaltonen *et al.* [CDF Collaboration], Phys. Rev. **D83** (2011) 112003 [arXiv:1101.0034 [hep-ex]].

- [20] [CDF Collaboration], CDF Note 9724.
- [21] T. Aaltonen *et al.* [CDF Collaboration], Phys. Rev. Lett. **101** (2008) 202001 [arXiv:0806.2472 [hep-ex]].
- [22] J. Weinelt, Masters thesis, Universität Karlsruhe, FERMILAB-MASTERS-2006-05; IEKP-KA-2006-21.
- [23] D. Hirschbuehl, Ph.D. Thesis, Universität Karlsruhe, FERMILAB-THESIS-2005-80.
- [24] T. A. Schwarz, Ph.D. Thesis, University of Michigan, FERMILAB-THESIS-2006-51, UMI-32-38081.
- [25] P. Ferrario, G. Rodrigo, Phys. Rev. **D80** (2009) 051701 [arXiv:0906.5541 [hep-ph]].
- [26] G. Rodrigo, P. Ferrario, Nuovo Cim. **C33** (2010) 04 [arXiv:1007.4328 [hep-ph]].
- [27] S. Jung, H. Murayama, A. Pierce, J. D. Wells, Phys. Rev. **D81** (2010) 015004 [arXiv:0907.4112 [hep-ph]].
- [28] K. Cheung, W. -Y. Keung, T. -C. Yuan, Phys. Lett. **B682** (2009) 287-290 [arXiv:0908.2589 [hep-ph]].
- [29] J. Shu, T. M. P. Tait, K. Wang, Phys. Rev. **D81** (2010) 034012 [arXiv:0911.3237 [hep-ph]].
- [30] S. Westhoff, Presented at HEP-EPS Grenoble 2011. [arXiv:1108.3341 [hep-ph]]
- [31] L. G. Almeida, G. F. Sterman, W. Vogelsang, Phys. Rev. **D78** (2008) 014008 [arXiv:0805.1885 [hep-ph]].
- [32] V. Ahrens, A. Ferroglia, M. Neubert, B. D. Pecjak, L. L. Yang, JHEP **1009** (2010) 097 [arXiv:1003.5827 [hep-ph]].
- [33] S. Dittmaier, P. Uwer, S. Weinzierl, Eur. Phys. J. **C59** (2009) 625-646 [arXiv:0810.0452 [hep-ph]].
- [34] S. Dittmaier, P. Uwer, S. Weinzierl, Phys. Rev. Lett. **98** (2007) 262002 [hep-ph/0703120].
- [35] W. Hollik, D. Pagani, [arXiv:1107.2606 [hep-ph]].
- [36] J. H. Kühn, A. Scharf, P. Uwer, Eur. Phys. J. **C51** (2007) 37-53 [hep-ph/0610335].
- [37] J. H. Kühn, A. Scharf, P. Uwer, Eur. Phys. J. **C45** (2006) 139-150 [hep-ph/0508092].
- [38] W. Bernreuther, M. Fucker, Z. G. Si, Int. J. Mod. Phys. **A21** (2006) 914-917 [hep-ph/0509210].
- [39] W. Bernreuther, M. Fuecker, Z. G. Si, Phys. Rev. **D74** (2006) 113005 [hep-ph/0610334].
- [40] W. Hollik, M. Kollar, Phys. Rev. **D77** (2008) 014008 [arXiv:0708.1697 [hep-ph]].
- [41] The Tevatron Electroweak Working Group [CDF and D0 Collaboration], [arXiv:1007.3178 [hep-ex]].
- [42] K. Nakamura *et al.* [Particle Data Group], J. Phys. G **37** (2010) 075021.

- [43] A. D. Martin, W. J. Stirling, R. S. Thorne and G. Watt, Eur. Phys. J. C **63** (2009) 189 [arXiv:0901.0002 [hep-ph]].
- [44] J. M. Campbell, R. K. Ellis, Phys. Rev. **D60** (1999) 113006 [hep-ph/9905386].
- [45] [CMS Collaboration], CMS-PAS-TOP-10-010, CMS-PAS-TOP-11-014.
- [46] [ATLAS Collaboration], ATLAS-CONF-2011-106.
- [47] R. Demina, Presented at HEP-EPS Grenoble 2011.
- [48] T. Sjostrand, S. Mrenna, P. Z. Skands, JHEP **0605** (2006) 026 [hep-ph/0603175].
- [49] P. Ferrario, G. Rodrigo, Phys. Rev. **D78** (2008) 094018 [arXiv:0809.3354 [hep-ph]].
- [50] P. Ferrario, G. Rodrigo, JHEP **1002** (2010) 051 [arXiv:0912.0687 [hep-ph]].
- [51] J. L. Hewett, J. Shelton, M. Spannowsky, T. M. P. Tait, M. Takeuchi, Phys. Rev. D **84** (2011) 054005 [arXiv:1103.4618 [hep-ph]].
- [52] G. Aad *et al.* [ATLAS Collaboration], [arXiv:1108.6311 [hep-ex]].
- [53] S. Chatrchyan *et al.* [CMS Collaboration], [arXiv:1107.4771 [hep-ex]].

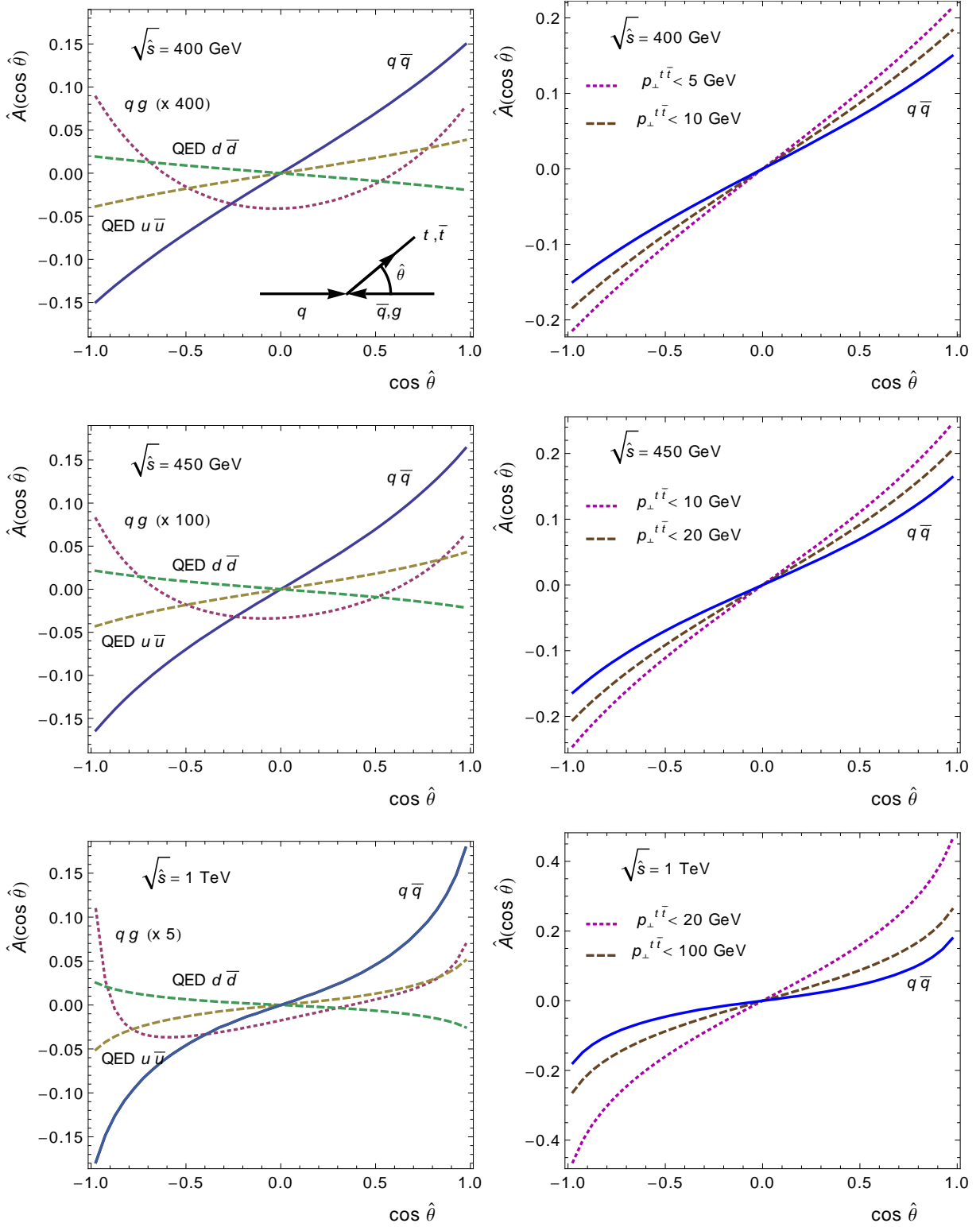


Figure 6: Left plots: differential partonic asymmetries from $q\bar{q}$ and qg induced events for different choices of the partonic center of mass energy. The asymmetry from mixed QED-QCD contributions is shown separately for u and d quarks. Right plots: differential partonic asymmetries after introducing a cut in the transverse momentum of the $t\bar{t}$ pair $p_{\perp}^{t\bar{t}}$.

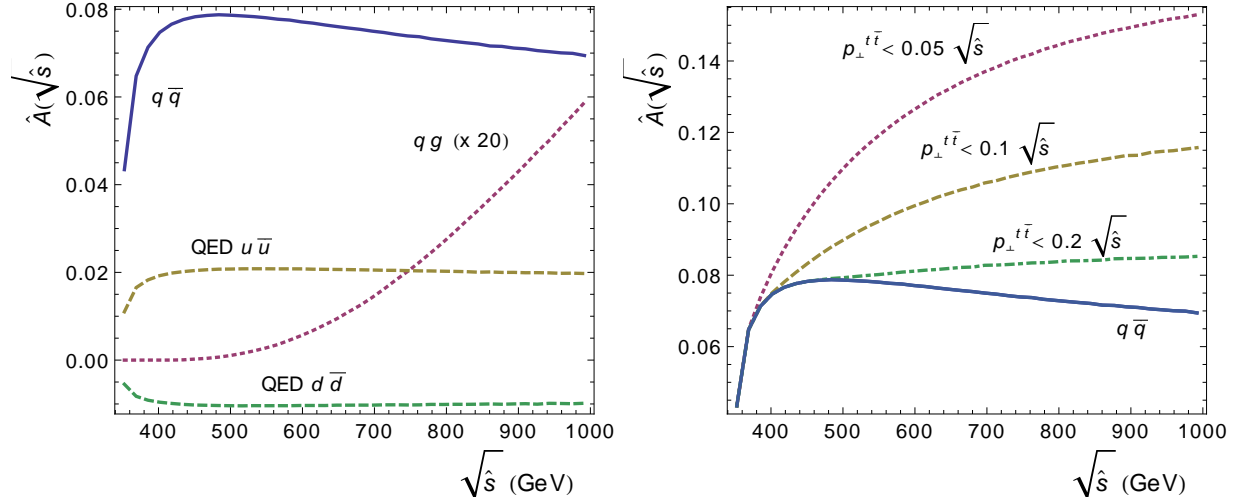


Figure 7: Left plot: integrated partonic asymmetry from $q\bar{q}$ and qg induced events for different choices of the partonic center of mass energy. The asymmetry from mixed QED-QCD contributions is shown separately for u and d quarks. Right plot: integrated partonic asymmetry after introducing a cut in the transverse momentum of the $t\bar{t}$ pair $p_{\perp}^{t\bar{t}}$.

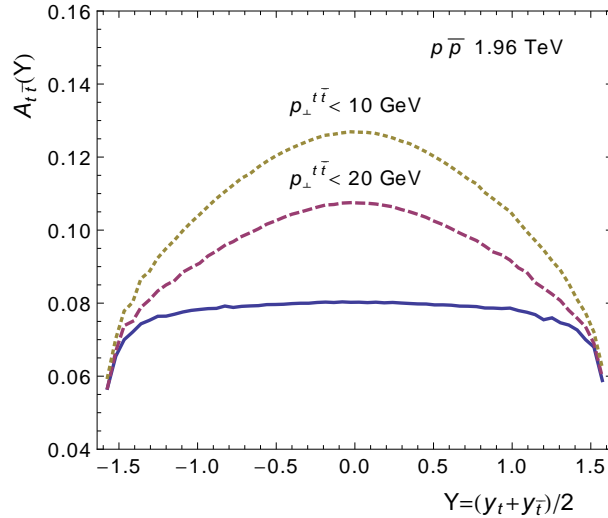


Figure 8: Rapidity dependence of the asymmetry $A_{t\bar{t}}(Y)$ as defined in Eq. (10). Solid line: no cut on $p_{\perp}^{t\bar{t}}$, dotted/dashed line $p_{\perp}^{\max} = 10$ GeV / 20 GeV.

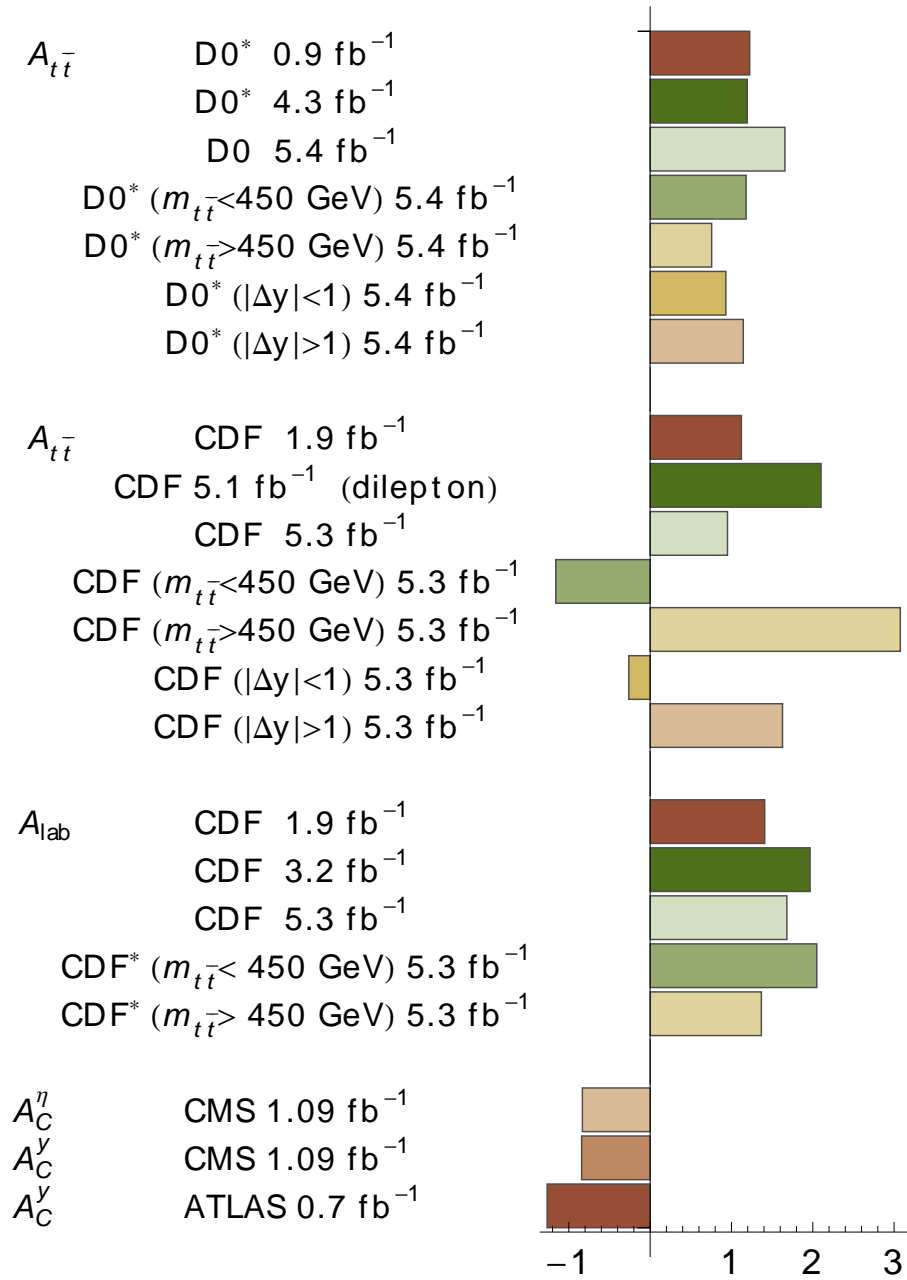


Figure 9: Summary of experimental measurements of the charge asymmetry in comparison with the SM theoretical predictions. The histogram represents the pull of the discrepancy for each measurement. The asterisk * indicate “reconstruction level” results, the others are parton level.

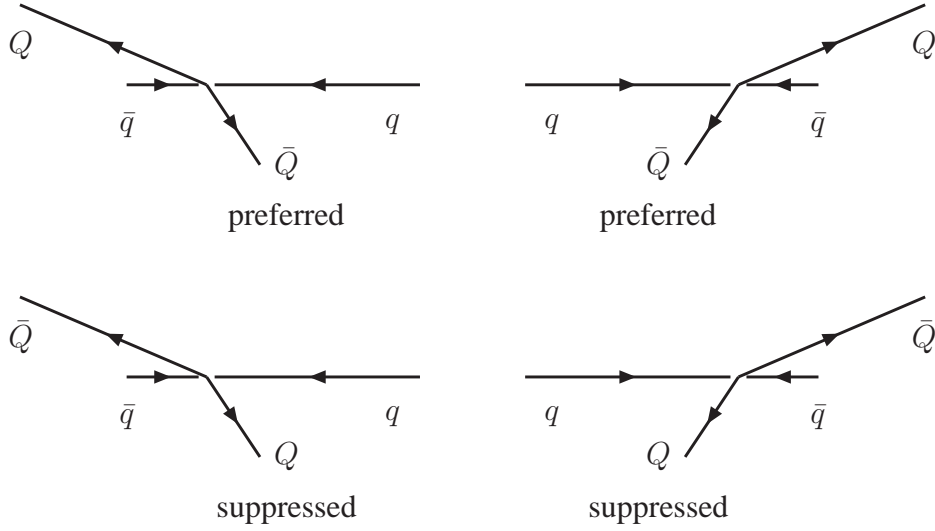


Figure 10: Preferred and suppressed configurations at the LHC.

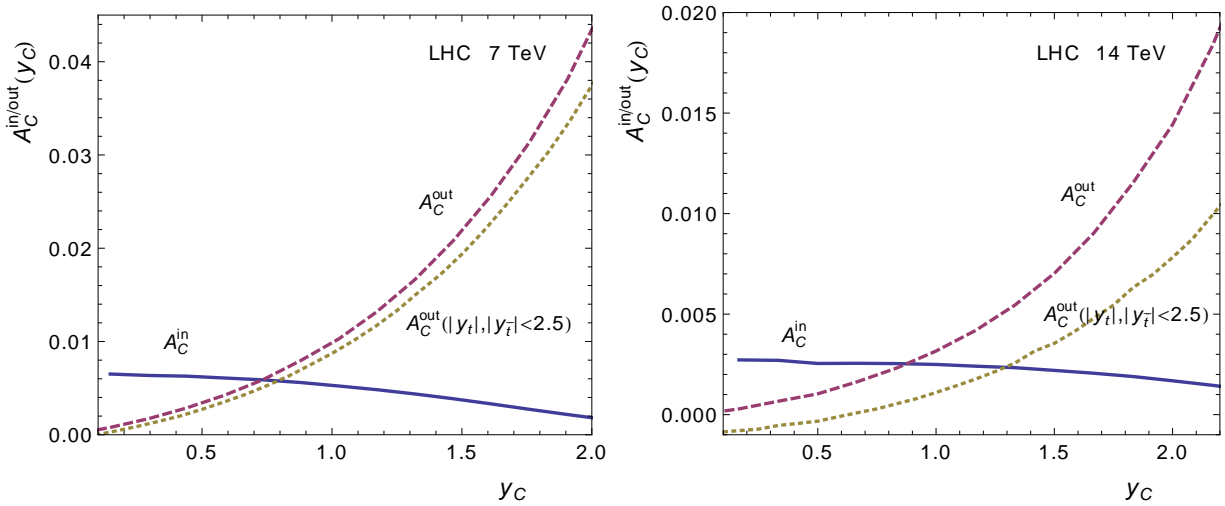


Figure 11: In and out charge asymmetries at the LHC with $\sqrt{s} = 7$ TeV and 14 TeV as a function of the cut y_C in rapidity. The out charge asymmetry $A_C^{out}(y_C)$ is also calculated with an upper cut in the rapidity of the top and anti-top quarks $|y_t|, |y_{\bar{t}}| < 2.5$.

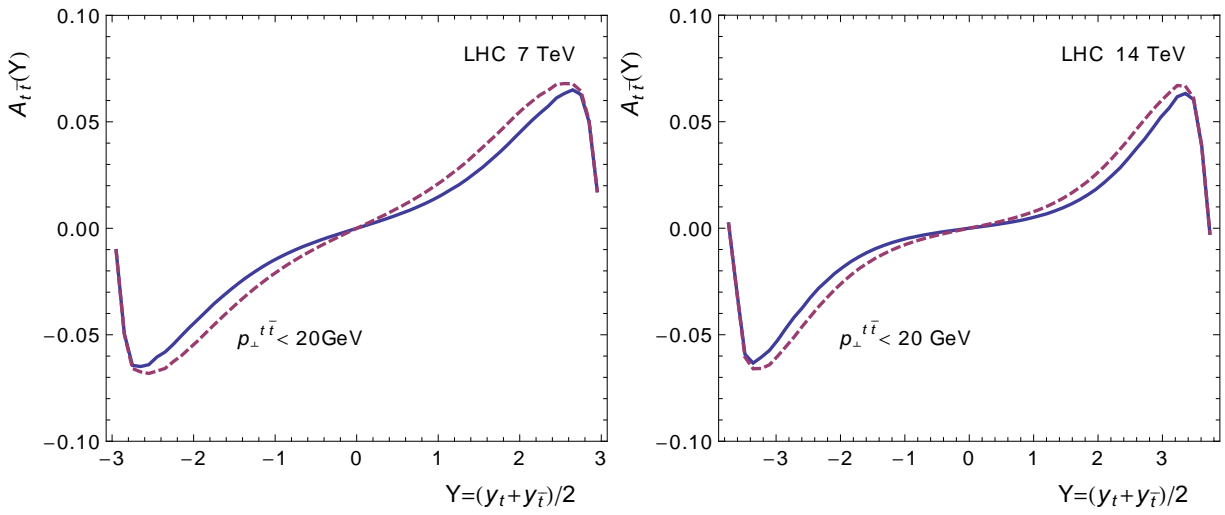


Figure 12: Pair charge asymmetry at the LHC with $\sqrt{s} = 7 \text{ TeV}$ and 14 TeV as a function of the mean rapidity $Y = (y_t + y_{\bar{t}})/2$. Solid line: no cut on $p_{\perp}^{t\bar{t}}$, dashed line: $p_{\perp}^{\text{max}} = 20 \text{ GeV}$.

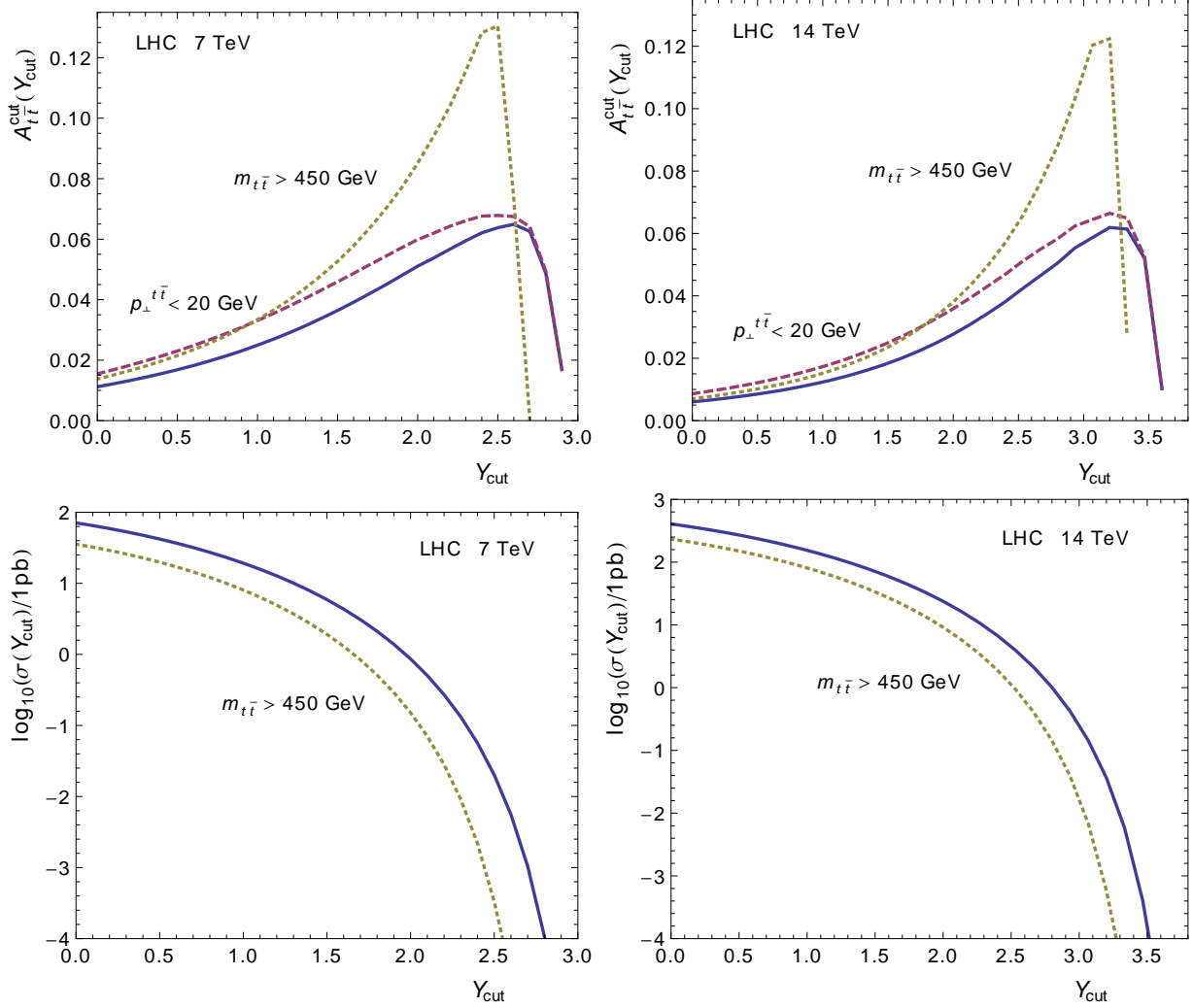


Figure 13: Integrated pair charge asymmetry and integrated cross-section as a function of Y_{cut} at the LHC with $\sqrt{s} = 7$ TeV and 14 TeV. Solid line: without extra cuts, dashed line: $p_{\perp}^{\text{max}} = 20$ GeV, dotted line: $m_{t\bar{t}} > 450$ GeV.

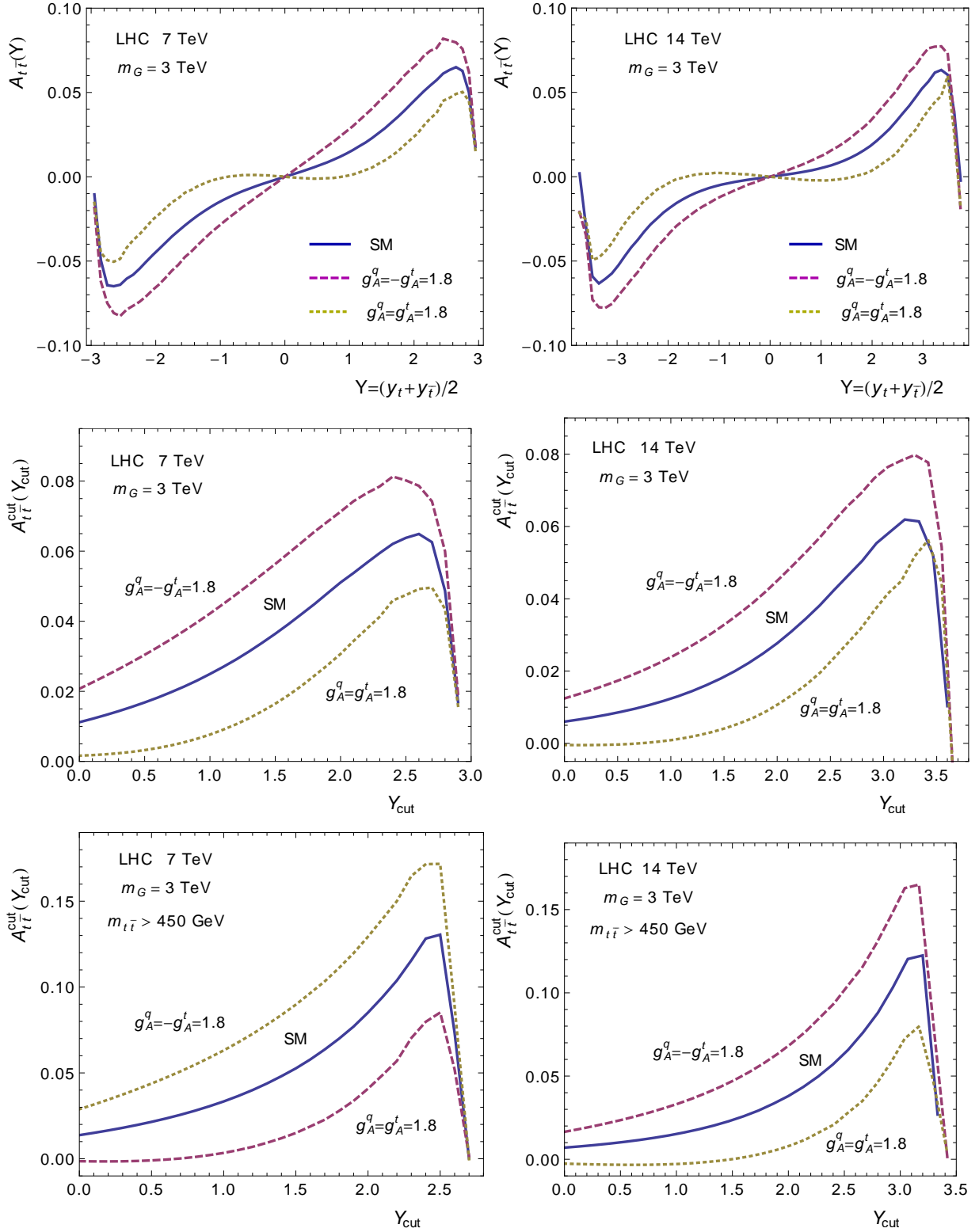


Figure 14: Pair charge asymmetry $A_{t\bar{t}}$ at the LHC as a function of the mean rapidity $Y = (y_t + y_{\bar{t}})/2$, and integrated pair charge asymmetry $A_{t\bar{t}}^{\text{cut}}$ as a function of Y_{cut} , with and without a cut in the invariant mass of the top quark pair $m_{t\bar{t}}$. Left plots with $\sqrt{s} = 7$ TeV and right plots with 14 TeV.